Characterizing liquid phase fabric of unsaturated specimens from X-ray computed tomography images

K.N. Manahiloh [1], B. Muhunthan [2]

[1 2] Department of Civil and Environmental Engineering, Washington State University, Pullman, WA-99164, USA

Abstract

Pore-water in the funicular and pendular saturation regimes of the SWCC ($S_r < 90\%$) assumes a complex fabric consisting of saturated pockets of water under negative pressure and a network of liquid bridges formed from menisci at the contact points of particles. Measurement and characterization of the liquid fabric for unsaturated soil assemblies over a range of saturation, stress, and deformation plays a pivotal role in improving our fundamental understanding of unsaturated soil behavior. However, lack of data collection as hindered the consideration of the liquid phase in relation to fabric distribution and evolution.

In this study X-ray CT imaging was conducted to monitor the changes in the liquid fabric of unsaturated glass beads over a wide range of saturation along drying and wetting paths. Images showing the three distinct phases of unsaturated specimens were successfully obtained. The anisotropic fabric distribution of liquid phase is characterized using tensors. A computer code that automatically analyzes multiple images to quantify the components of a second-order fabric tensor was developed and applied to CT images obtained along the drying and wetting paths of a SWCC determined by digital image processing. Principal values, principal directions and invariants are quantified and implications of the changes to better description of unsaturated soil behavior are discussed.

Keywords: Unsaturated soil; Microfocus X-ray CT; Anisotropy; Fabric tensor; granular geomaterial; SWCC.

Citation information: Please cite this work as follows

Manahiloh, K.N. and B. Muhunthan. *Characterizing Liquid Phase Fabric of Unsaturated Specimens from X-Ray Computed Tomography Images*. in *Unsaturated Soils: Research and Applications*. 2012. Berlin, Heidelberg: Springer Berlin Heidelberg.

1. Introduction

Unsaturated soil mechanics plays a key role in a range of natural earth processes and engineered earth systems. Flow related problems (e.g. water balance at soil-atmosphere interface, surface contaminant transport, transient and steady seepage in unsaturated embankment dams, landfill covers and liners), stress related problems (e.g. precipitation-induced slope stability failures, bearing capacity and settlement of shallow foundations, excavation and borehole stability, stress wave propagation) and deformation related problems (e.g. expansive or collapsing soils, settlement and consolidation of unsaturated soil and soil compaction) are a few examples impacted by engineering properties of unsaturated soils (Lu and Likos 2004). Despite the importance of unsaturated soils in geotechnical engineering practice, implementation of their mechanics in modeling, measuring and predicting behavior is limited. Although considerable research has been conducted in recent years (e.g. Fredlund and Rahardjo 1993; Likos and Lu 2004; Lu and Likos 2004; Matyas and Radhakrishna 1968; Nemat-Nasser 1982; Ng and Menzies 2007), continuing advances are crucial to fully incorporate unsaturated soil mechanics into engineering practice.

In the funicular and pendular saturation regimes of unsaturated granular media - zones of the soil water characteristic curve (SWCC) in which the degree of saturation (S_r) is less than about 90% - the pore-water is characterized by a complex fabric consisting of saturated pockets of water under negative pressure and a network of liquid bridges formed from menisci at the contact points of particles (see Figure 1). Characterization of this fabric over a range of saturation, stress, and deformation should aid in understanding unresolved fundamental issues in of unsaturated soil behavior.

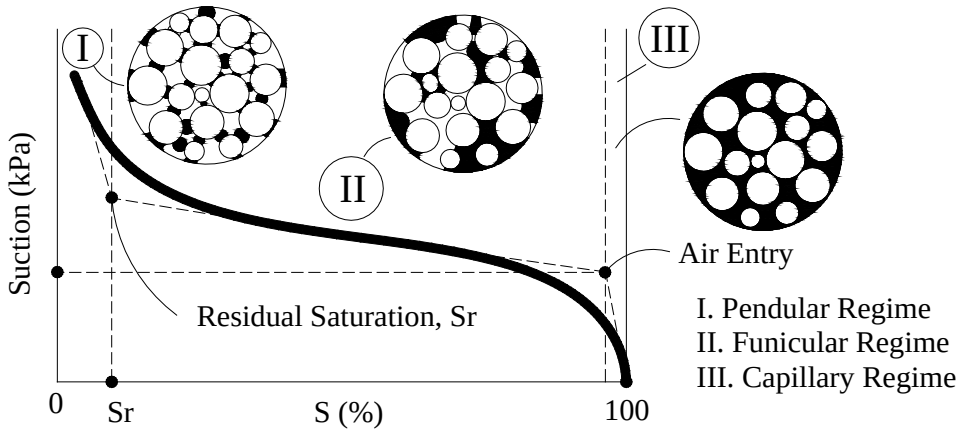

Fig.1. Regimes of SWCC for partially saturated granular soil

Nondestructive imaging techniques such as X-ray computed tomography (CT) have provided superior tools to quantitatively describe the 3-D microstructure of granular materials (e.g. Alshibli et al. 2000; Desruses et al. 1996; Gebrenegus et al. 2006; Wang et al. 2003). Combining X-ray CT scanning, digital image processing and criteria for approximating distributions one can extract directional data and characterize microstructure of partially saturated specimens.

The objective of this study is to automate the handling of liquid fabric in X-ray CT images of unsaturated specimens and obtain the fabric tensor of the liquid phase. Accordingly, directional data gathered from X-ray CT scanning of 1mm glass beads at different suctions are digitally analyzed. The present interest is not to treat the complete theory covering unsaturated specimens, but rather to exemplify the use of image processing in quantifying directional data for phases of interest and thus combine the technique with statistical correlations that describe phase distribution.

2. Fabric tensor of the liquid phase

The orientation of a surface, characterized by the direction of its normal vector, can be obtained from observation of phases of interest in a material. Even though, extracting directional information is a key step in understanding fabric distribution, interpretation in terms of given control factors proves a more crucial question. In their studies, Eringen (1962) and Truesdell & Noll (1965) commented the then existing statistical theories on directional data to have paid a little attention in describing physical problems with physical laws. Cowin (1978) asserted that particle packing influences the mechanical behavior of granular materials and claimed the convenience of using scalar parameters like porosity or void ratio as first measures of fabric. However, Oda (1972b), Arthur et al. (1977) and Symes et al. (1984) showed samples prepared with same porosity manifest different strength characteristics. Muhunthan (1991) discussed porosity as insufficient descriptor of fabric and suggested the necessity to introduce higher measures that represent the directional nature of granular soils. These measures were referred to as “second measures”. In attempts to describe fabric tensor mathematically, “fabric” had been defined by different researchers (e.g. Mitchell 1976; Muhunthan 1991; Scott 1963). Here fabric is accepted as a term referring to parameters like size, shape and arrangement of the solid particles, the organic inclusions and the associated voids which independently or in association will play important role in governing the behavior of soils.

In geomaterials, geometrical anisotropy is introduced by the preferential orientation of non-spherical particles that may evolve as a result of shearing deformations. Moreover the voids (liquid phase included) take irregular shapes and distribution. A tensor quantity has been introduced by earlier researchers (e.g. Kanatani 1984; Oda and Nakayama 1989) to express anisotropy that may arise from the solid phase of geomaterials. Recent decade has seen an

increased use of the concept of fabric tensor in representing particulate media and relating anisotropy with geometric distribution of phases. The studies have focused primarily on the possibility of finding effective continuum representation in terms of the micro-scale quantities whereby the geometry of the microstructure is admitted. The parameters obtained from such approaches were applied in plasticity and thermo-mechanical theories (e.g. Muhunthan 1991).

Most of the earlier researchers conducted their studies of fabric tensor on solid particles (e.g. Cowin and Satake 1978; Kanatani 1984; 1985; Mitchell 1976; Nemat-Nasser and Mehrabadi 1983; Satake 1982). To characterize solid particles, Oda and Nakayama (1989) followed Kanatani's definition of fabric tensor for two dimensional cases by defining a unit vector along the longest axis of the particles. According to Muhunthan (1991), defining tensor parameters on the void phase have a potential of delivering a unified measure for all particulate media. The use of second order measure on void phase will not only extend critical state soil mechanics concepts in a natural sense but also avoid the difficulty of defining contact normal, contact vector and their distribution in clayey and silty particles. Moreover, the advent of X-ray CT and its application to scanning of geomaterials has enabled to distinctly image the solid, liquid, and gas phases at a microstructural level. This enhanced capability should help in understanding the liquid phase contributions to structural anisotropy. Statistical correlations applicable to solid particles are assumed to appropriately describe directional distributions on the liquid phase. Following the preceding discussion, this study will quantify higher measures of fabric on the liquid phase of a partially saturated specimen.

3. Mathematical background for fabric tensor

Kanatani (1984) sought tensor quantities that characterize directional distribution of particles and gave expressions for fabric tensors of three kinds. The subsequent discussion

revises the mathematical formulations developed, on distribution of directional data and fabric tensors, by the captioned author.

If $f(n)$ is assumed to be the "empirical" distribution density of the observed directional data, then it can easily be shown that $\int f(n)dn = 1$. In the integral, dn is the differential solid angle which is given as:

$$\int dn = \int_0^{\pi} \int_0^{2\pi} \sin\theta d\phi d\theta \qquad \text{(For three dimensional cases)} \tag{1}$$

$$\text{And} \quad \int dn = \int_0^{2\pi} d\theta \qquad \text{(For two dimensional cases)} \tag{2}$$

The singular distribution function, $f(n)$ is approximated by a smooth function F(n) to estimate the "true" population distribution in such a way that a "model" or "parametric form" is first assumed and then some form of "Measure of Approximation" between two distributions is introduced. Typical parametric forms of F(n) suggested by Kanatani (1984) are given in Equations 3 through 5. These forms respectively represent a polynomial in n, a non negative polynomial and an exponential family.

$$F(n) = C + C_i n_i + C_{ij} n_i n_j + C_{ijk} n_i n_j n_k + \ldots \tag{3}$$

$$F(n) = [C + C_i n_i + C_{ij} n_i n_j + C_{ijk} n_i n_j n_k + \ldots]^2 \tag{4}$$

$$F(n) = \exp[C + C_i n_i + C_{ij} n_i n_j + C_{ijk} n_i n_j n_k + \ldots] \tag{5}$$

Typical forms of criteria as introduced by Kanatani are given in Equations 6 through 8. Equation 7 represents the least square approximation. This criterion, when applied on the polynomial parametric form, turns to the spherical harmonic expansion in 3-D and the Fourier series expansion in 2-D. Equation 7 is referred to as the "Hellinger distance" approximation and Equation 8 represents the "Kullback Information" also known as "Entropy". All of these forms are invariant to coordinate transformation and hence have invariant meanings.

i. The least square error approximation:

$$\int [F(n) - f(n)]^2 dn \rightarrow Minimum \tag{6}$$

ii. The "Hellinger Distance" approximation:

$$\int [\sqrt{F(n)} - \sqrt{f(n)}]^2 dn \rightarrow Minimum \tag{7}$$

iii. The "Kullback Information":

$$-\int f(n) \log \frac{f(n)}{F(n)} dn \rightarrow Maximum \tag{8}$$

Assuming a pair of unit vectors with opposite directions are to be generated so that *f(n)*is a symmetric function with respect to the origin, Equations 3 and 6 can be combined such that the square error *E* is minimized, to obtain the following form.

$$E = \int [(C + C_{ij} n_i n_j + C_{ijkl} n_i n_j n_k n_k + ...) - f(n)]^2 dn \rightarrow Minimum \tag{9}$$

Note that contraction of $n_i n_j n_k n_l$ over $k = \ell$ yields $n_i n_j$ and further contraction over $i = j$ yields 1. Moreover, symmetry of the function allows omitting the odd powers of *n***.** But, the coefficients (C_i) are not unique as 1, $n_i n_j$, $n_i n_j n_k n_\ell$ are linearly dependent.

Kanatani (1984) approximated distribution functions for solid particles and gave expressions for fabric tensors of the "first", "second" and "third" kind as expansions of relevant subspaces. In three dimensional subspaces (i.e. vector space of functions on S^2 spanned by $n_{i_1} \ldots n_{i_n}$ and dimension $(n+1)(n+2)/2$), the distribution function approximations are as given in Equations 10, 12 and 14 while equations 11, 13 and 15 represent the associated fabric tensors.

$$f(n) = \frac{1}{N} \sum_{\alpha=1}^{N} \delta(n - n^{(\alpha)}) \tag{10}$$

$$N_{i_1 i_2 \ldots i_n} = \left\langle n_{i_1} n_{i_2 \ldots} n_{i_n} \right\rangle \text{ (Fabric tensor of "first" kind or the "Moment tensor")} \tag{11}$$

$$f(n) = \frac{1}{4\pi} F_{i_1 \ldots i_n} n_{i_1 \ldots} n_{i_n} \tag{12}$$

$$F_{i_1 i_2 \ldots i_n} = \frac{2n+1}{2^n}\binom{2n}{n}[N_{i_1 i_2 \ldots i_n} + a^n_{n-2}\delta_{(i_1 i_2} N_{i_3 \ldots i_n)} + a^n_{n-4}\delta_{(i_1 i_2}\delta_{i_3 i_4} N_{i_5 \ldots i_n)} + a^n_0 \delta_{(i_1 i_2}\delta_{i_3 i_4}\ldots\delta_{i_{n-1} i_n)}] \quad (13)$$

$$f(n) = \frac{1}{4\pi}[1 + D_{ij} n_i n_j + D_{ijkl}\, \mathrm{n}_i\, n_j n_k n_l + \ldots] \quad (14)$$

$$D_{i_1 \ldots i_n} = \frac{2n+1}{2^n}\binom{2n}{n}[N_{i_1 \ldots i_n}] \quad (15)$$

In Equation 10, $\delta(n - n^{(\alpha)}) = \delta(\theta - \theta^{(\alpha)})\delta(\phi - \phi^{(\alpha)})/\sin\theta^{(\alpha)}$ and $\delta(n - n^{(\alpha)}) = \delta(\theta - \theta^{(\alpha)})$ represent the Dirac Delta function in 3-D (i.e. $n^{(\alpha)} = (\sin\theta^{(\alpha)}\cos\theta^{(\alpha)}, \sin\theta^{(\alpha)}\sin\theta^{(\alpha)}, \cos\theta^{(\alpha)})$ or spherical coordinate) and 2-D (i.e. $n^{(\alpha)} = (\cos\theta^{(\alpha)}, \sin\theta^{(\alpha)})$ or polar coordinate) spaces.

In two dimensional subspaces i.e. vector space of functions on S spanned by $n_{i_1} \ldots n_{i_n}$ and dimension ***n***+1, the distribution function approximations for fabric tensors of the "second" and the "third" kind will be modified and are as given in Equations 16 and 18 respectively while equations 17 and 19 represent the associated fabric tensors.

$$f(n) = \frac{1}{2\pi} F_{i_1 \ldots i_n} n_{i_1 \ldots} n_{i_n} \quad (16)$$

$$F_{i_1 i_2 \ldots i_n} = 2^n[N_{i_1 i_2 \ldots i_n} + a^n_{n-2}\delta_{(i_1 i_2} N_{i_3 \ldots i_n)} + \ldots + a^n_0 \delta_{(i_1 i_2}\delta_{i_3 i_4}\ldots\delta_{i_{n-1} i_n)}] \quad (17)$$

$$f(n) = \frac{1}{2\pi}[1 + D_{ij} n_i n_j + D_{ijkl}\, \mathrm{n}_i\, n_j n_k n_l + \ldots] \quad (18)$$

$$D_{i_1 \ldots i_n} = 2^n N_{\{i_1 \ldots i_n\}} \quad (19)$$

The fluctuation of the density function is better accounted for and its distribution is accurately represented when higher order tensors are used. However, for mathematical convenience, terms up to second tensor (i.e. $n = 2$) are assumed to be sufficient descriptors of the distribution (e.g. Muhunthan 1991). Thus, in three dimensional subspaces, for $n = 2$, the

expressions for Kanatani's tensors of the "second" and "third" kind reduce to Equation 20 and 21 respectively. The corresponding tensor definitions in two dimensional subspaces are given by Equations 22 and 23.

$$F_{ij} = \frac{15}{2}[N_{ij} - \frac{1}{5}\delta_{ij}] \tag{20}$$

$$D_{ij} = \frac{15}{2}[N_{ij} - \frac{1}{3}\delta_{ij}] \tag{21}$$

$$F_{ij} = 4[N_{ij} - \frac{1}{4}\delta_{ij}] \tag{22}$$

$$D_{ij} = 4[N_{ij} - \frac{1}{2}\delta_{ij}] \tag{23}$$

4. Experimental setup

X-ray CT scanners allow visualization of the interior of objects by capturing digital information on their 3-D microstructure (e.g. Denison et al. 1997; Masad et al. 1999). Accordingly, X-ray computed tomography (CT) imaging is performed at Washington State University (WSU) using a cone beam X-ray FlashCT (Flat Panel Amorphous Silicon High Resolution Computed Tomography) machine. The facility is a novel design that incorporates an X-Tec 225 keV microfocus X-ray source and a flat-panel Varian PaxScan 2520 detector equipped with CsI scintillator capable of accommodating resolutions as high as 5 μm for specimens with sizes on the orders of a millimeter to centimeter. This X-ray CT system, shown as Figure 2 and Figure 3, can be thought as composed of four subgroups. The first group consists of the energy source assemblies with DC generators and X-ray sources. The X-ray control panel and cooling system may be regarded as the control unit assembly. The group of equipments composed of central workstation and multiple processors can be referred to as processing assembly and the scanning unit assembly with elements of a detector, specimen stage and frame

grabber is the fourth subgroup. As part of this study, soil specimens are scanned under controlled suction to capture the three-phase fabric (i.e. solid, liquid and gas).

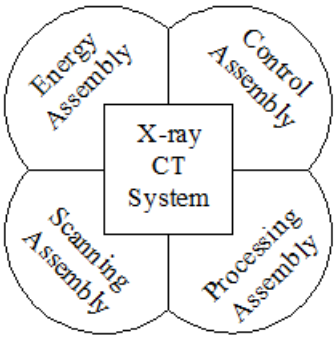

Fig. 2. X-ray Computed Tomography system (CT-system) at Washington State University

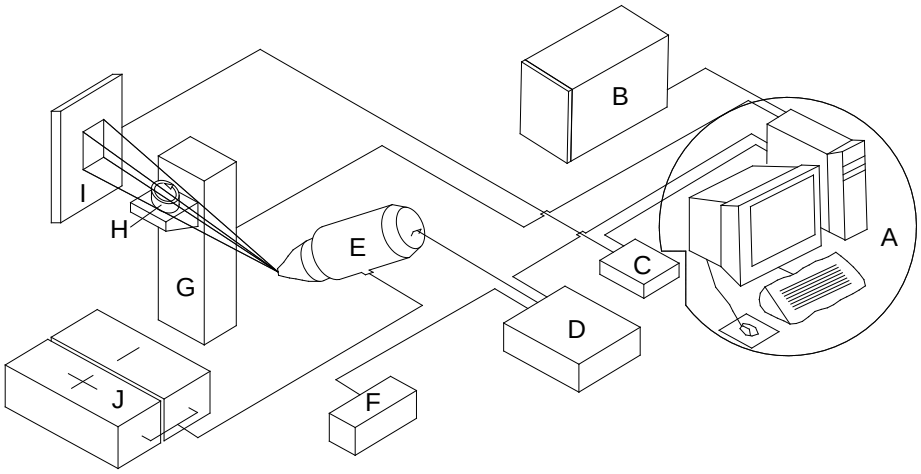

Fig. 3. Schematics of X-ray Computed Tomography (CT) system at Washington State University: (A) Central workstation; (B) Processer; (C) Frame grabber; (D) X-ray control; (E) X-ray source; (F) Cooling system; (G) Stage; (H) Sample; (I) Detector; (J) DC generators.

The least square error approximation is adopted as a measure of criteria. Focus is given to testing uniformly-graded round glass beads with particle diameter of 1.0 mm. The selection was made to ensure application of low magnitude matric suction (i.e. attainable in labs with hanging column technique) to bring samples to degree of saturations representing the capillary, funicular, and pendular regimes and obtain high resolution images for the chosen specimen size thereby allowing to effectively distinguish and accurately quantify the grain, pore-air, and pore-fluid features. Analytical operations are applied to X-ray CT images in which the liquid phase was

distinctively captured by doping the saturating fluid with 6% CsCl solution. Since the CT system used has cone beam geometry, Feldkamp's approximation for three dimensional filtered back projections is adopted for image reconstruction. X-ray CT images of unsaturated samples, such as shown in Figure 4, are analyzed to extract directional data. Results from digital image processing are utilized in computing the components of second order fabric tensors that describe directional distributions for liquid component of the three-phase unsaturated system. Invariants of the computed fabric tensors are then calculated following existing correlations.

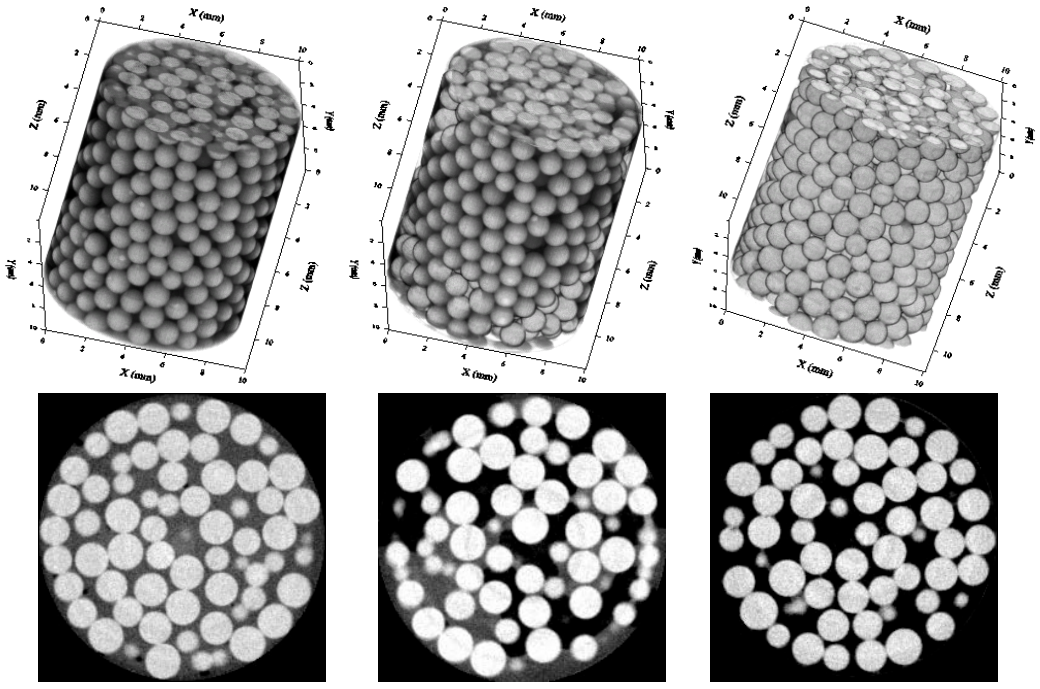

(a) (b) (c)

Fig. 4. 3-D and 2-D images for some of the specimens used in quantifying fabric tensor: (a) fully saturated slice; (b) partially saturated slice; (c) dry slice

To illustrate the techniques applied a hypothetical two dimensional image is considered in Figure 5. The horizontal and vertical axes are represented by x_1 and x_2 respectively. In figure 5, $n^{(k)}$ represents a unit vector aligned with the longest chord of the k^{th} "particle" and θ is its inclination angle with respect to the horizontal axis. As long as good contrast shows clear images

of the liquid phase, the definition of the term "particle" need not necessarily be limited to the solids.

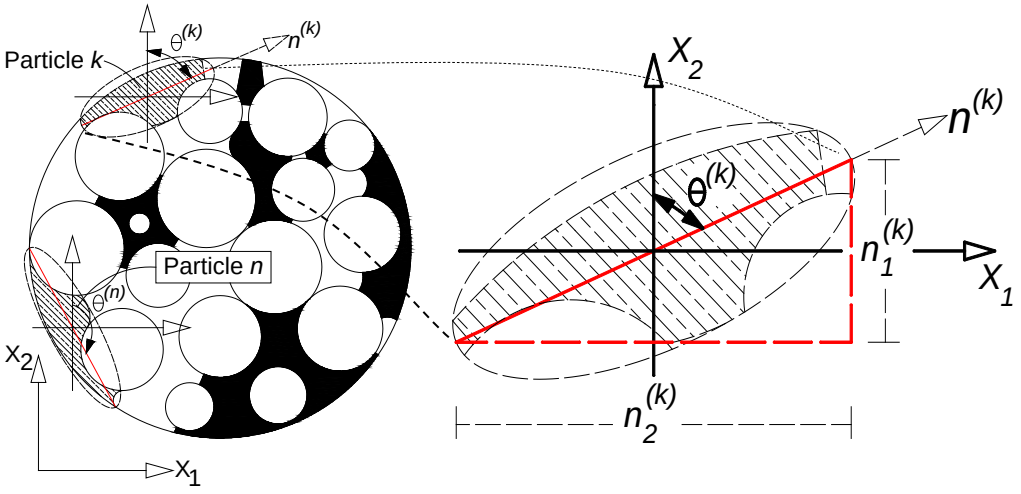

Fig. 5. Two dimensional section showing orientation of particles: (a) Image from CT scanning with local and global axes; (b) k^{th} Liquid particle with longest chord and fitting ellipsoid in 2-D.

Decomposing the unit vector into its orthogonal components, one can obtain expressions for n_1 and n_2 as follows:

$$n_1 = \sin\theta^{(k)} \text{ and } n_2 = \cos\theta^{(k)} \tag{24}$$

In each X-ray CT image, the total number of data points (i.e. each liquid completely or partially surrounded by solid particles) for which directional data is to be sought is represented by M. According to Oda and Nakayama (1989), for such two dimensional cases, the components of the fabric tensor can then be calculated as:

$$N_{11} = \frac{1}{M}\sum_{k=1}^{M}\sin^2\theta^{(k)} \tag{25}$$

$$N_{12} = \frac{1}{M}\sum_{k=1}^{M}\cos\theta^{(k)}\sin\theta^{(k)} \tag{26}$$

$$N_{22} = \frac{1}{M}\sum_{k=1}^{M}\cos^2\theta^{(k)} \tag{27}$$

Image Pro Plus platform is used to run a macro that handles the direction assignment, angle measurement and computations for components of the fabric tensor. A typical image from X-ray CT scanning is shown in Figure 6a. Figure 6b shows AutoCAD simulation of the same image where the three independent phases (i.e. solid, liquid and gas) are represented with green, red and black colors respectively. In Figure 7a the gas phase is isolated out and shown shaded in black. Figure 7b shows the longest chords of liquid phases. Similar images for the liquid phase are shown in Figure 8a and 8b.

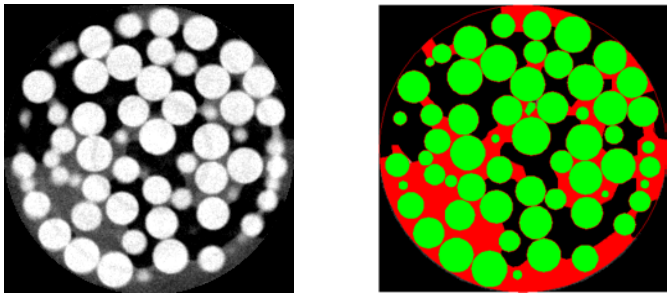

(a) (b)

Fig. 6. Image from X-ray CT: (a) 1mm Glass Bead at suction of 0.6kPa (Drying); (b) All Phases: AutoCAD Simulation in which Black = Gas, Red = Liquid and Green = solid.

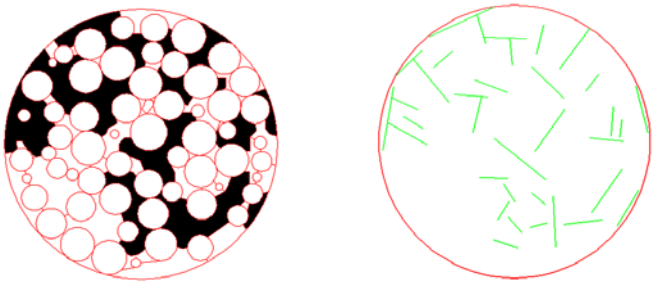

(a) (b)

Fig. 7. The gas Phase: (a) AutoCAD Simulation (black = gas); (b) Longest chord representation for gas phase.

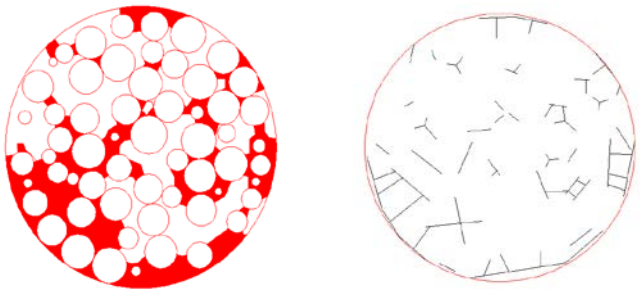

(a) (b)

Fig. 8. The liquid Phase: (a) AutoCAD Simulation (red = liquid); (b) Longest chord representation for liquid phase.

The automated program works in such a way that the written macro identifies the liquid phase based on the appropriate threshold values and assigns longest possible chord on each liquid particle. Then it quantifies the direction of each liquid particle and from that angle, calculates the components of the fabric tensor from Equations 25 through 27.

The samples considered for the analysis are summarized in Table 1. Columns 2 and 3 of the table present the sizes of the sample in pixels and in millimeters. To relate measurements on images to actual measurements, the calculation macro requires calibration of the images. These values are shown as column 5 in the table. The cropping coordinates and the threshold ranges used to guide the program to identify liquid particles are given in columns 6 and 7 respectively.

Table 1. Sample details

(1)	(2)	(3)		(4)	(5)	(6)	(7)
Sample	**Suction (kPa)**	**Diameter**		**Height (mm)**	**Calibration mm/pixel**	**Cropping coordinates**	**Threshold for Liquid**
		pixel	**mm**				
1	0.0	236	10	14.32	0.042	(0,0;236,236)	31-127
2	0.4	236	10	13.97	0.042	(0,0;236,236)	31-127
3	0.6	234	10	14.58	0.043	(0,0;234,234)	31-127
4	0.8	271	10	11.95	0.037	(0,0;271,271)	31-127
5	2.5	238	10	13.98	0.043	(0,0;238,238)	31-127

5. Results and Discussion

To calculate the values of N_{11}, N_{12} and N_{22}, equations 25, 26 and 27 are coded in a macro and the obtained results for sample 1 are shown in figures 7 through 9.

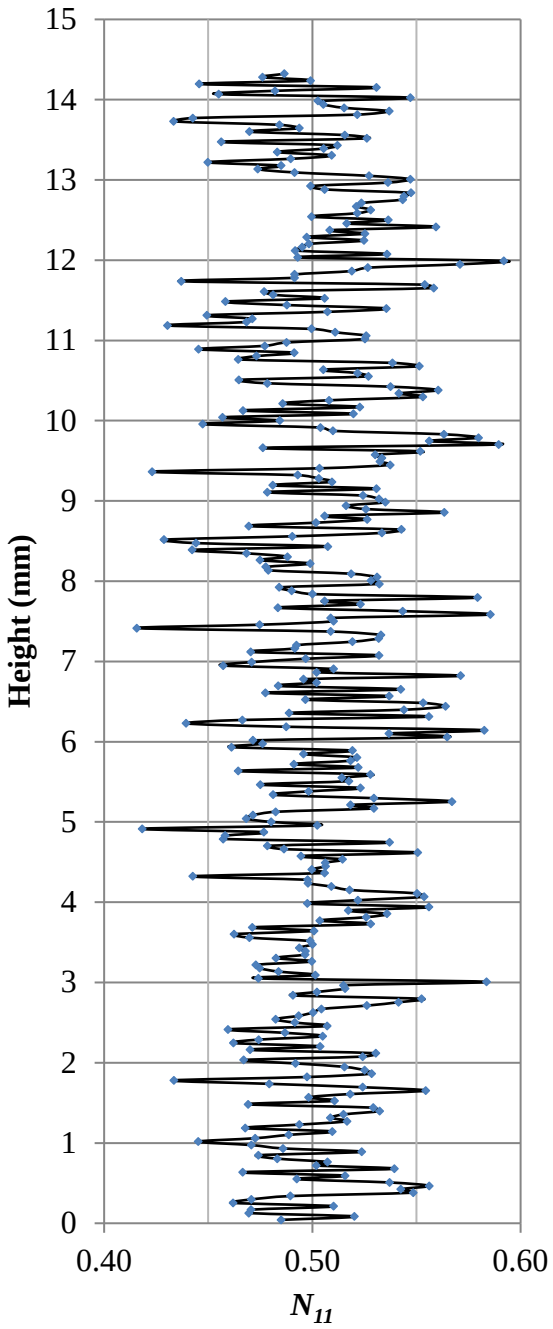

Fig. 9. N_{11} distribution over the height of sample 1 (0.0kPa)

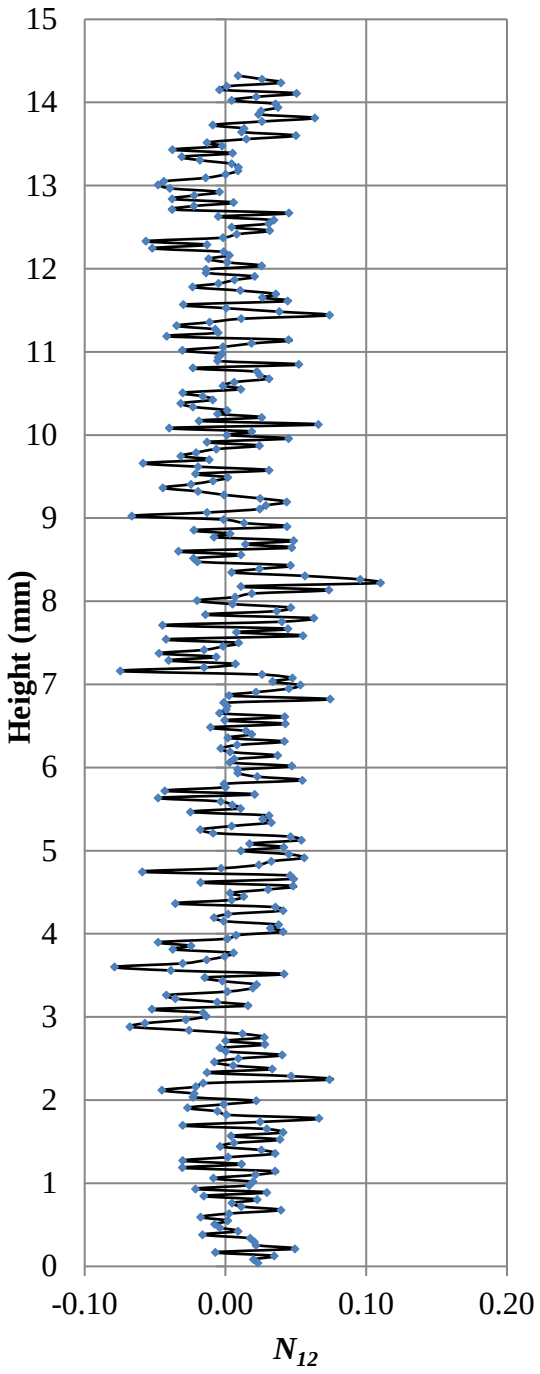

Fig. 10. N_{12} distribution over the height of sample 1 (0.0kPa)

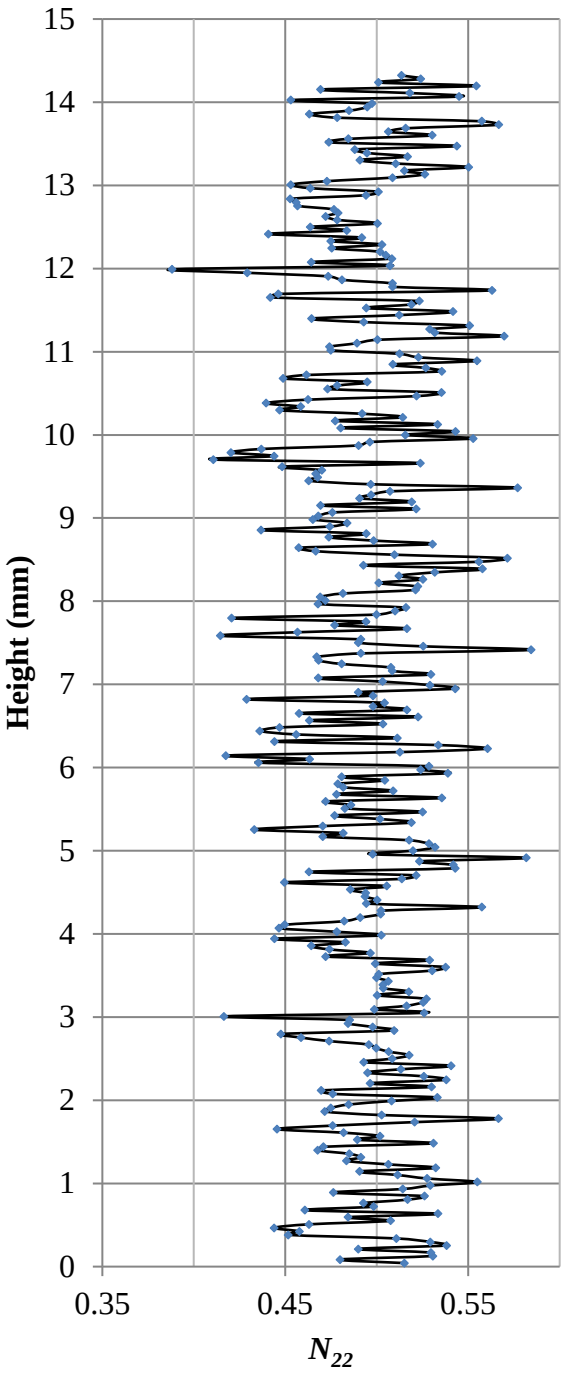

Fig. 11. N_{22} distribution over the height of sample 1 (0.0kPa)

Average values for the distribution descriptors and their invariants are summarized in Table 2. From the values indicated, the fundamental property of fabric tensors can be proven such that the first invariant, I_1, is always Unity. Moreover it can be observed that the second invariant remains constant throughout. The invariants are plotted together to show their variation as a function of the sample preparation pressure.

Table 2. Average Values for N_{ij} and associated Invariants.

Sample	**Suction** (kPa)	**N_{11}**	**N_{12}**	**N_{22}**	***I_1***	***I_2***
1	0	0.504	0	0.496	1.000	0.250
2	0.4	0.503	0	0.497	1.000	0.250
3	0.6	0.506	0	0.494	1.000	0.250
4	0.8	0.512	0	0.488	1.000	0.250
5	2.5	0.502	0	0.498	1.000	0.250

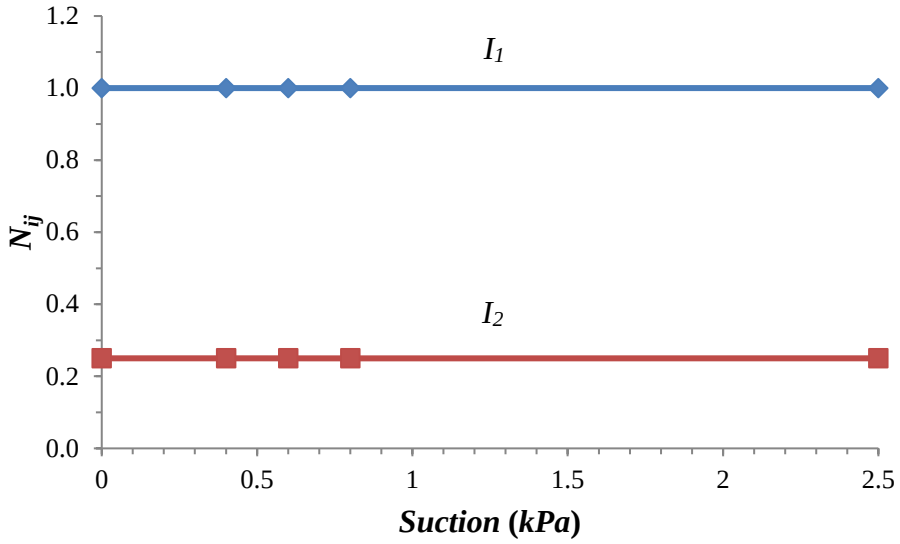

Fig. 12. Average N_{ij} values for all samples

Following the previous assertion, N_{ij} is written in full as a symmetric second order tensor and as an example the values for sample 1 are indicated below.

$$\begin{bmatrix} N_{11} & N_{12} \\ N_{21} & N_{22} \end{bmatrix} = \begin{bmatrix} 0.504 & 0 \\ 0 & 0.496 \end{bmatrix}$$

Since N_{ij} is a symmetric second order tensor, the components can be converted to two principal values N_1 and N_3 in the corresponding principal directions. The mathematical formulations to do so, and the corresponding principal directions, are given in Equations 28 and 29. Also, the tensor invariants can be computed as for any other tensor quantities.

$$\begin{bmatrix} N_1 \\ N_2 \end{bmatrix} = \frac{1}{2}[N_{11} + N_{22}] \pm \left[\frac{1}{4}(N_{11} - N_{22}) + {N_{12}}^2 \right]^{1/2} = \frac{1}{2}(1 \pm \Delta) \tag{28}$$

$$\begin{bmatrix} \theta_1 \\ \theta_2 \end{bmatrix} = \frac{1}{2} \arctan \frac{2N_{12}}{N_{22} - N_{11}} \tag{29}$$

Curray (1956) introduced the term denoted by Δ in Equation 29 and named it "the vector magnitude." It is an index measure that shows the intensity of a preferred orientation of particles and can be quantified as given in equation 30.

$$\Delta = \frac{1}{M} \left[\sum_{k=1}^{M} \left(\cos 2\theta^{(k)} \right)^2 + \sum_{k=1}^{M} \left(\sin 2\theta^{(k)} \right)^2 \right]^{1/2} \tag{30}$$

The results for the principal values, principal directions and the vector magnitude values are summarized in table 3. Note that all are average values as they are given based on averaged values of N_{ij}.

Table 3. Principal values, principal directions and vector magnitudes.

Sample	N_{11}	N_{12}	N_{22}	N_1	N_2	Δ	θ_1	θ_2
1	0.504	0	0.496	0.546	0.454	0.091	0	90
2	0.503	0	0.497	0.537	0.463	0.074	0	90
3	0.506	0	0.494	0.556	0.444	0.111	0	90
4	0.512	0	0.488	0.579	0.421	0.157	0	90
5	0.502	0	0.498	0.531	0.469	0.061	0	90

Now, for two dimensional cases, the relationship between F_{ij} (Kanatani's fabric tensor of the "second" kind) and D_{ij} (Kanatani's fabric tensor of "third" kind) with N_{ij} can be obtained by applying equations 22 and 23 (i.e. $D_{ij} = 4\left[N_{ij} - \frac{1}{2}\delta_{ij} \right]$ and $F_{ij} = 4\left[N_{ij} - \frac{1}{4}\delta_{ij} \right]$).

Note also that the principal components of F_{ij} and D_{ij} can be derived from same relationships. Employing representation of equation 28, the principal components takes the form indicated by equations 31 and 32. The resulting values are given in tables 4 and 5.

$$\begin{bmatrix} D_1 \\ D_2 \end{bmatrix} = \pm 2\Delta \tag{31}$$

$$\begin{bmatrix} F_1 \\ F_2 \end{bmatrix} = 1 \pm 2\Delta = 1 + \begin{bmatrix} D_1 \\ D_2 \end{bmatrix} \tag{32}$$

Table 4. Kanatani's fabric tensor of the "second" kind

Sample	**F_{11}**	**F_{12}**	**F_{22}**	**F_1**	**F_2**	**Δ**
1	1.017	0	0.983	1.184	0.816	0.092
2	1.011	0	0.989	1.148	0.852	0.074
3	1.025	0	0.975	1.222	0.778	0.111
4	1.049	0	0.951	1.314	0.686	0.157
5	1.007	0	0.993	1.124	0.876	0.062

Table 5. Kanatani's fabric tensor of the "third" kind

Sample	**D_{11}**	**D_{12}**	**D_{22}**	**D_1**	**D_2**	**Δ**
1	0.017	0	-0.017	0.184	-0.184	0.092
2	0.011	0	-0.011	0.148	-0.148	0.074
3	0.025	0	-0.025	0.222	-0.222	0.111
4	0.049	0	-0.049	0.314	-0.314	0.157
5	0.007	0	-0.007	0.124	-0.124	0.062

6. Conclusions

Both second order fabric descriptors given by Kanatani (1984) (i.e. fabric tensor of the "second" and "third" kind) are successfully quantified, in an automated manner, for the liquid phase component of unsaturated specimens from X-ray CT scanned images. The fabric tensor components have satisfied the basic tensorial properties of symmetry and equality of diagonal summation to unity. The principal values, principal directions, and vector magnitudes for the liquid fabric of the considered samples are derived from the fabric tensor components which in turn are obtained by digital processing of high resolution X-ray CT images. The technique is non destructive and this feature makes it a profound alternative for further studies.

References

Alshibli, K. A., Sture, S., Costes, N. C., Frank, M. L., Lankton, M. R., Batiste, S. N., and Swanson, R. A. (2000). "Assessment of Localized Deformation in Sand Using X-Ray Computed Tomography." *Geotechnical Testing Journal*, 23(3), 274-299.

Arthur, J. R. F., Chua, K. S., and Dunstan, T. (1977). "Induced Anisotropy in a Sand." *Geotechnique*, 27(1), 13-30.

Cowin, S. C., and Satake, T. (1978). Continuum mechanical and statistical approaches in the mechanics of granular materials, Gakujutsu Bunken Fukyu-Kai, Tokyo, Japan.

Curray, J. R. (1956). "Analysis of two-dimensional orientation data." *Jour. Geology.*, 64, 117-131.

Denison, C., Carlson, W. D., and Ketcham, R. A. (1997). "Three-Dimensional Quantitative Textural Analysis of Metamorphic Rocks Using High-Resolution Computed X-Ray Tomography: Part I. Methods and Techniques." *Journal of Metamorphic Geology*, 15(29-44).

Desruses, J., Chambron, R., Mokni, M., and Mazerolle, F. (1996). "Void Ratio Evolution inside Shear Brands in Triaxial Sand Specimen Studied by Computed Tomography." *Geotechnique*, 46(3), 529-546.

Eringen, A. C. (1962). *Nonlinear Theory of Continuous Media* McGraw-Hill, New York.

Fredlund, D. G., and Rahardjo, H. (1993). *Soil Mechanics for unsaturated soils*, John Wiley and Sons Inc., New York.

Gebrenegus, T., Tuller, M., and Muhunthan, B. "The Application of X-ray computed tomography for characterization of surface crack networks in sand-bentonite mixtures." *Advances in X-ray tomography for geomaterials*, 207-212.

Kanatani, K. I. (1984). "Distribution of Directional Data and Fabric Tensors." *International Journal of Engineering Science*, 22, 149-164.

Kanatani, K. I. (1985). "Procedures for stereological estimation of structural anisotropy." *International Journal of Engineering Science*, 23(5), 587-598.

Likos, W. J., and Lu, N. (2004). "Hysteresis of capillary stress in unsaturated granular soil." *Journal of Engineering Mechanics*, 130(6), 646-655.

Lu, N., and Likos, W. J. (2004). *Unsaturated soil Mechanics* Wiley, New Jersey.

Masad, E., Muhunthan, B., Shashidhar, N., and Harman, T. (1999). "Internal Structure Characterization of Asphalt Concrete Using Image Analysis." *Journal of Computing in Civil Engineering, ASCE*, 13(2), 88-95.

Matyas, E. L., and Radhakrishna, H. S. (1968). "Volume change characteristics of partially saturated soils " *Geotechnique*, 18(4), 432-448 .

Mitchell, J. K. (1976). *Fundamentals of soils behavior*, John Wiley and sons, Inc., New York, N.Y.

Muhunthan, B. (1991). "Micromechanics of Steady State, Collapse and Stress-Strain Modeling of Soils," Perdue University, West Lafayette, 221pp.

Nemat-Nasser, S. "Fabric and its influence on mechanical behaviour of granular materials." *IUTAM Conference on deformation and failure of granular materials, Delft*, Delft, 37-42.

Nemat-Nasser, S., and Mehrabadi, M. M. (1983). "Stress and Fabric in Granular Masses." in: Mechanics of Granular Materials: New Models and Constitutive Relations, J. T. Jenkins and M. Satake, eds., Elsevier, Amsterdam, 1-8.

Ng, W. W., and Menzies, B. (2007). *Advanced Unsaturated Soil Mechanics and Engineering*, Taylor & Fransis, New York.

Oda, M. (1972b). "The Mechanism of Fabric Changes during Compressional Deformation of Sand." *Soils and Foundations*, 12(2), 1-18.

Oda, M., and Nakayama, H. (1989). "Yield Function for soil with Anisotropic Fabric." *Journal of Engineering Mechanics*, 115(1), 89-104.

Satake, M. (1982). "Fabric tensor in Granular Materials." IUTAM Symposium on Deformation and Failure of Granular Materials Delft, 63-68.

Scott, R. F. (1963). "Principles of soil mechanics." Addison-Wesley Publishing Co. Inc., Massachusetts, 267-275.

Symes, M. J., Gens, A., and Hight, D. W. (1984). "Undrained Anisotropy and Principal Stress Rotation in Saturated Sand." *Geotechnique*, 34(1), 11-27.

Truesdell, C., and Noll, W. (1965). "The Non-Linear Field Theory of Mechanics." Handbuch der. Physik, III/3, S. Flugge, ed., Springer-Verlag Berlin.

Wang, L. B., Frost, J. D., Voyiadjis, G. Z., and Harman, T. P. (2003). "Quantification of damage parameters using X-ray tomography images." *Mechanics of Materials*, 35, 777-790.